CDF/ANAL/TOP/PUB/11092

Forward-backward asymmetry in $b\bar{b}$ pairs at high mass

The CDF Collaboration

(Dated: June 3, 2014)

Abstract

We measure the forward-backward asymmetry in $b\bar{b}$ pairs at large $b\bar{b}$ mass using jet-triggered data and jet charge to identify b from $\bar{b}$. As a function of $m_{b\bar{b}}$, the asymmetry is consistent with zero, with standard model predictions, and with some new physics predictions. We exclude an axigluon with a mass of $200\,\mathrm{GeV}\,c^{-2}$, restricting the parameter space available to light axigluon models for the $t\bar{t}$ asymmetry.

PACS numbers: 14.65.Ha

CONTENTS

I. INTRODUCTION

In recent years, measurements of the forward-backward asymmetry (A_{FB}) of top-quark pair production at the Tevatron proton-antiproton collider at Fermilab have been consistently larger [1] than predicted by the standard model [2, 3]. Further study of this phenomenon has led to a number of proposed models of new physics [4]. One specific class of models is the low-mass axigluon [5]. These models include a new, heavy, axial-vector boson with a mass below the $t\bar{t}$ threshold and a width broad enough to evade detection in light-quark resonance searches. A potentially sensitive test of such models is to study the forward-backward asymmetry of pair production of other quark flavors, such as bottom.

TABLE I. Results of calculation by Grinstein and Murphy [6]. Cuts match our analysis cuts: $|\eta_{b,\bar{b}}| < 1.1$.

$m_{b\bar{b}}$ [GeV c^{-2}]	$A_{\rm FB}(b\bar{b})$ [%]
$[150, 225]$	$2.2 \pm 0.7 \pm 0.2$ %
$[225, 325]$	$4.2 \pm 1.3^{+0.6}_{-0.5}$ %
$[325, 1960]$	$7.8 \pm 2.3^{+1.7}_{-1.4}$ %

II. THEORETICAL EXPECTATIONS

At a hadron collider $b\bar{b}$ production is almost exclusively a QCD process. The vast majority of $b\bar{b}$ production is due to gluon-gluon fusion, which has no asymmetry due to the symmetric initial state. We are principally interested in measuring the $q\bar{q} \to b\bar{b}$ asymmetry, so we will have to select a kinematic region where the quark-antiquark initial state is significantly enhanced over the symmetric gluon-fusion background. Since there are more quarks at large Bjorken x, one way to achieve this $q\bar{q} \to b\bar{b}$ selection is to go to large $m_{b\bar{b}}$.

Several theorists have computed the SM prediction for $A_{\rm FB}(b\bar{b})$ at high mass, with varied answers [2, 3, 6]. Kuhn and Rodrigo [2] compute that the asymmetry for $b\bar{b}$ pairs with $\sqrt{\hat{s}} \leq 300\,{\rm GeV}$ and $|\cos\,| < 0.9$ is in the range 4.3 % to 5.1 %. Manohar and Trott [3] compute $A_{\rm FB}(b\bar{b})$ in several bins of $m_{b\bar{b}}$. They find $A_{\rm FB}(b\bar{b}) = 0.4\,\%$ inclusively and $A_{\rm FB}(b\bar{b})$ =7.8 % to 8.1 % for $350 < m_{b\bar{b}} < 650\,{\rm GeV}\,c^{-2}$, depending on the choice of scale. Grinstein and Murphy [6] have the most comprehensive calculation, and have tuned their calculation to match our analysis cuts. The results of this calculation are summarized in Table I.

III. TRIGGERING AND EVENT SELECTION

The data used for this analysis was collected online using inclusive jet triggers. We use three transverse energy thresholds, requiring at least one jet with $E_T > 50$, 70, and $100\,{\rm GeV}\,c^{-2}$. The two lower-threshold triggers only accept one event out of 100 or eight, respectively. After data-quality requirements and trigger prescales, we analyze $95\,{\rm pb}^{-1}$, $1.2\,{\rm fb}^{-1}$, and $9.5\,{\rm fb}^{-1}$ of integrated luminosity, respectively.

The offline event selection requires at least two jets [7] with $E_T > 20\,{\rm GeV}$ and rapidity $|y| < 2$. Of the jets which pass these cuts, exactly two must contain a secondary vertex

consistent with the decay of a b quark (b tagged), identified using a secondary vertex identification algorithm (SECVTX) [8]. The invariant mass $m_{b\bar{b}}$ of the two b-tagged jets must be at least $150\,\mathrm{GeV}\,c^{-2}$.

IV. METHODOLOGY

The forward-backward asymmetry A_{FB} for fermion-antifermion production is defined as

$$A_{FB} = \frac{N_F - N_B}{N_F + N_B} \tag{1}$$

where N_F is the number of events where the fermion is forward of the antifermion in rapidity ($y = y_b - y_{\bar{b}}$) and N_B the number where it is backward. This definition using rapidity is invariant under boosts along the beam axis. Events with $y > 0$ are considered forward and those with $y < 0$ are considered backward. We identify the fermion and the antifermion using the momentum-weighted average of the charges of the tracks associated with each jet,

$$Q_{jet} = \frac{\sum_t q_t(\vec{p}_t \cdot \vec{p}_{jet})^{0.5}}{\sum_t(\vec{p}_t \cdot \vec{p}_{jet})^{0.5}}, \tag{2}$$

where the sum t is over all tracks in the jet, q_t is the charge of the track, and $\vec{p}_t$ and $\vec{p}_{jet}$ are the momentum vectors of the track and the jet, respectively.

As discussed in Section II, the asymmetry depends strongly on the mass of the $b\bar{b}$ pair, both in the SM and in models with an axigluon. In order to fully understand the A_{FB}, we must divide our sample into several ranges of $m_{b\bar{b}}$. Our choice of $m_{b\bar{b}}$ bins is motivated by our online event selection. Each jet energy trigger threshold efficiently selects events only over a limited range of $m_{b\bar{b}}$. Events with $150 < m_{b\bar{b}} < 225\,\mathrm{GeV}\,c^{-2}$ are selected with a jet transverse energy threshold of 50 GeV, and the thresholds of 70 and 100 GeV are used to select events with $m_{b\bar{b}}$ in the ranges $225 < m_{b\bar{b}} < 325$ and $325\,\mathrm{GeV}\,c^{-2} < m_{b\bar{b}}$, respectively.

The definition in (1) presumes that N_F and N_B can be measured without any background, detector effects, or forward-backward confusion. In practice, we must accommodate many such effects, such as backgrounds and the dilution of the asymmetry due to misidentifying fermions as antifermions and vice-versa. We therefore extend the definition of A_{FB} to

$$A_{FB} = \frac{1}{2P-1}\frac{(N_F - N_F^{bkgd}) - (N_B - N_B^{bkgd})}{N_F + N_F^{bkgd} + N_B + N_B^{bkgd}}, \tag{3}$$

where N_F and N_B are the observed numbers of events, N_F^{bkgd} and N_B^{bkgd} are the estimated numbers of background events, and P is the probability to make the fermion/antifermion

assignments correctly. These are not the only effects we must contend with, and we employ a Bayesian technique to relate the $A_{\rm FB}$ and these systematic effects to the number of measured forward and backward events. This is described in detail in section IV E.

A. Sample purity

We estimate the fraction of events where both b-tagged jets are true b jets by counting events where one or both of the secondary vertices are on the opposite side of the primary vertex from the jet direction. These "negative" tags are predominantly fake tags from light-flavor jets and are a product of the finite position resolution of the tracking system. We expect there to be an equal number of fake tags from this source on the default, "positive" side, together with additional contributions of fake tags from K_S/Λ and interactions with the detector material which are not present in the negative tags [9].

We compute the number of true $b\bar{b}$ events using

$$N_{b\bar{b}} = \frac{1}{\xi}(N_{++} - \lambda N_{+-} + \lambda^2 N_{--}) \tag{4}$$

Where N_{++} is the number of observed positive double-tag events, N_{+-} is the number of events with one of the tags negative, N_{--} is the number with both tags negative, and ξ is a factor defined in (5). This relation can be understood by considering N_{+-} as the number of events with either one b-tag and one fake tag or two fake tags. The two fake tag case will be double-counted by this estimate, because there are two permutations for which jet is the positive tag and which is the negative tag. Therefore the N_{--} term which is an estimate of the number of two fake tag events is added to correct for the double-counting. The λ factors are inserted to correct the negative tag rates into estimates of the total positive fake tag rates. Their determination will be described later in this section.

The factor ξ in (4) is inserted to correct for the presence of b jets in the negative tags. Its value is

$$\xi = 1 - 2\lambda r + \lambda^2 r^2, \tag{5}$$

here $r = \epsilon_b^-/\epsilon_b^+$ is the ratio of the negative to positive tag efficiencies for b jets. The value of r is estimated from Monte Carlo simulation.

Finally we must correct (4) for a two-flavor system, with only b jets and light-flavor jets. The data also include charm jets, so that $N_{b\bar{b}}$ is in some sense the number of $b\bar{b}$ and $c\bar{c}$ events

summed together. This tends to bias the number high. To correct for this we make the same purity measurement in both the data and MC to get a data/MC scale factor, which we then apply to the MC truth $b\bar{b}$ purity from the MC.

To improve the statistical power of the data, we split it into subsamples of varying $b\bar{b}$ purity and analyze them separately. The splitting is based on the distance between the primary and secondary vertex. We define two tag types with low (L) and high (H) significance. We are then left with three subsamples: LL (both tags L), LH (one L and one H tag), and HH (two H tags). The HH sample will have the highest $b\bar{b}$ purity, followed by LH and then LL with the lowest purity.

We measure the ratio of positive to negative light-flavor tag rates λ using the technique described in Ref. [9]. Because the Monte Carlo indicates no strong dependence of λ on jet E_T, we use the same measured values for all three dijet mass bins.

The method works by fitting the invariant mass distribution of the identified SECVTX tags m_{VTX}, and is designed to minimize dependence of the modeling of the negative tags by the simulation. The first step is to fit for the flavor composition of the "net" tagged sample. By "net", we mean the result of subtracting the m_{VTX} distribution of the negative b tags from that for the positive b tags. We do this both for the data and for three templates derived from the simulation, for b, c, and light-flavor jets. At this stage the net distribution should include only tags of real displaced vertices, as the symmetric component from tracking errors has been subtracted. In the case of light-flavor jets the real displaced vertices are those from Λ/K_S decays and interactions with the detector material.

The results of the fits of the three templates to the net data are shown in Figure 1. We perform two fits, one for L-tagged data and one for H-tagged. In the L-tagged sample we find that 20 % of the tags are charm and 60 % are bottom, with the remainder light-flavor. In the H-tagged sample we find 15 % charm and 50 % bottom.

With the net flavor fractions in hand we can use the full MC fit templates and the number of net tags in the data to predict the number of negative tags we expect from each flavor. Comparing that sum to the observed negative tags in the data, we find that the negative tags in the simulation must be scaled by 1.53 (L tags) or 1.29 (H tags) to match the data. We perform this scaling on the negative tags and correspondingly increase the positive tags by the same amount because of our assumption that the tracking-error component of the mistags represented by the negative tags should be symmetric.

FIG. 1. Fits of the net m_{VTX} distribution, for L (left) and H (right) tagged data.

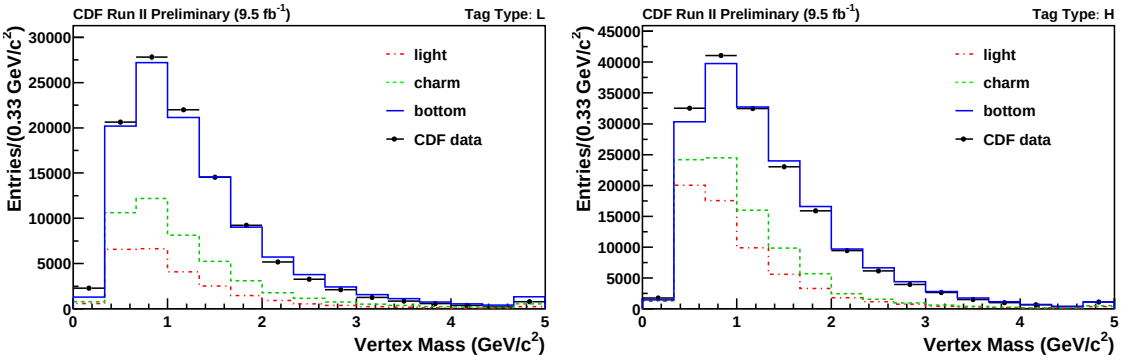

Using the numbers of positive and negative tags for light-flavor jets we can compute the λ factors needed for the b-fraction calibration. For the L tag we obtain 1.17 and for the H tag 2.98. These can be compared with the values from the simulation of 1.26 and 3.56. As expected, the values in the simulation are higher because it underestimates the negative tag rate. We also use these results to obtain a scale factor for the ratio of negative to positive b-jet tag rates, r, described above. In the simulation we find r values of 0.162 (L) and 0.0245 (H), while in the data we obtain 0.228 and 0.0314. Taking the ratios we find scale factors of 1.41 (L) and 1.28 (H) which are applied to the r values found from the simulation in each of the three mass bins.

Now that we have estimates for the numbers of background events in each sample, we also need to estimate the forward-backward asymmetry of the background, so that we know how many background events are forward and how many are backward.

B. Identification of the b jet using jet charge

The forward/backward assignment is performed using the momentum-weighted track charge, or "jet charge", for each of the two tagged jets. Distributions of the jet charge (Q_{jet}) for b jets and $\bar{b}$ jets are shown in Figure 2. Ultimately we use the difference of the two jet charges

$$Q = Q_1 - Q_2 \tag{6}$$

to make the assigment. If Q is negative that means the jet with charge Q_1 is the b jet, otherwise if Q is positive then the jet with charge Q_2 is the b jet.

In order to calibrate the performance of the jet charge algorithm from the data, we do

FIG. 2. Distributions of jet charge.

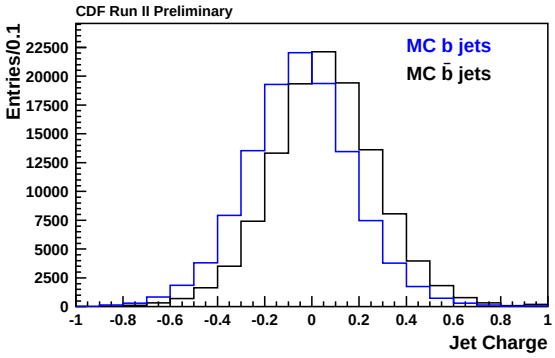

FIG. 3. Background asymmetry estimates, for 150-225 GeV (left), 225-325 GeV (right), and >325 GeV (bottom).

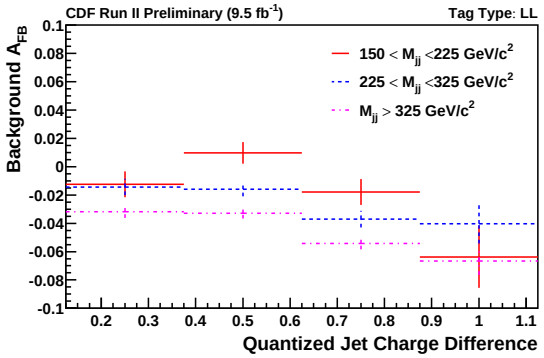

not use the full distribution but instead split it into discrete bins. The bin edges are -0.25, 0, and 0.25, so that there are a total of four bins. We assign Q_{jet} values of -0.5, -0.25, 0.25, and 0.5 to the bins. This translates into five bins of Q with values 0, 0.25, 0.5, 0.75, and 1.0. The bin with $Q = 0$ is not useful because it gives no indication how to assign the b jet, so only four bins of Q are used.

C. Background model

The non-$b\bar{b}$ background includes a wide variety of physics processes, including b+mistag, $u\bar{u}$, $d\bar{d}$, gluon jets, etc. Of primary concern here are scattering of valence quarks which, because they can proceed through the t-channel, exhibit a forward-backward asymmetry. Rather than attempt to tune the simulation to reproduce all of these processes in the proper sizes, we use data in a sideband selection that we expect to be enhanced in background and depleted of $b\bar{b}$ signal. This sideband employs a looser version of the SECVTX b-tagging

algorithm, where at least one of the tagged jets is a negative tag.

The asymmetry of the background is always negative, indicating that $u/\bar{u}$ scattering is the most important component. The u quark tends to follow the incoming proton direction in t-channel scattering which would indicate a postive A_{FB}, but the opposite charge of the u and b quark, combined with our definition of the asymmetry in terms of the jet charge, reverses the sign of the asymmetry.

D. Charge-identification probability

We also require an estimate of the probability P to have correctly chosen the b jet. We calibrate this from the data using the fraction of the events where the two Q_{jet} values have opposite sign. The two values which we are trying to measure are $p_{0.25}$, the probability for a jet with $Q_{jet} = 0.25$ to be a b jet (or for $Q_{jet} = -0.25$ to be a $\bar{b}$ jet), and $p_{0.5}$ defined similary for the jets with $|Q_{jet}| = 0.5$.

We start by measuring the number of opposite-charge events, N_{OC}, and number of same-charge events, N_{SC}, in the data in each dijet mass bin. These numbers are corrected for background using the calibrated b-fractions and the double-loose-tagged background model. We assume that what remains is $b\bar{b}$, not bb or $\bar{b}\bar{b}$ and compute $F_{OC} = N_{OC}/(N_{OC} + N_{SC})$.

In events where both jets have $|Q_{jet}| = 0.25$, the opposite-sign fraction can be expressed as

$$F_{OC}^{0.25-0.25} = p_{0.25}^2 + (1 - p_{0.25})^2 \tag{7}$$

which can be intuitively understood since the Q_{jet} measurements either both have the correct sign or both have the wrong sign. Similarly,

$$F_{OC}^{0.25-0.5} = p_{0.25}p_{0.5} + (1 - p_{0.25})(1 - p_{0.5}) \tag{8}$$

$$F_{OC}^{0.5-0.5} = p_{0.5}^2 + (1 - p_{0.5})^2 \tag{9}$$

for events with one of each Q_{jet} value and events with both jets with $|Q_{jet}| = 0.5$. We measure each F_{OC} in the data and solve for $p_{0.5}$ and $p_{0.25}$. These numbers are per-jet probabilities, and need to be converted to per-event probabilities to be used in the analysis. This is done

using the following expressions

$$P_{0.25} = \frac{p_{0.5}(1-p_{0.25})}{p_{0.5}(1-p_{0.25}) + (1-p_{0.5})p_{0.25}} \tag{10}$$

$$P_{0.5} = \frac{p_{0.25}^2}{p_{0.25}^2 + (1-p_{0.25})^2} \tag{11}$$

$$P_{0.75} = \frac{p_{0.25}p_{0.5}}{p_{0.25}p_{0.5} + (1-p_{0.25})(1-p_{0.5})} \tag{12}$$

$$P_{1.0} = \frac{p_{0.5}^2}{p_{0.5}^2 + (1-p_{0.5})^2} \tag{13}$$

where the subscript of P indicates the Q value of the bin.

E. Correction to hadron-jet level

In order to compare our result with theory and with other experimental results, we need to correct for acceptance and mismeasurement. The bulk of the mismeasurement effect is from jet-charge mismeasurement, and is handled by the analyzing power correction already discussed. The remaining effect of mismeasurement is due variously to jet energy mismeasurement and jet direction mismeasurement.

Jet energy mismeasurement principally affects the measurement of the dijet mass. Since we use very wide mass bins, this effect is small but not negligible. Jet direction mismeasurement only matters for very small y, and can cause forward events to appear backward and vice versa. We estimate all mismeasurement effects using Monte Carlo simulation. See Figure 4 for the effect of mismeasurement on the measured dijet mass.

We also estimate the effect of the potentially asymmetric acceptance of our detector and analysis selection. We apply our analysis event selection to the simulated events. From this, we can estimate the fraction of forward events (ϵ_F) and the fraction of backward events (ϵ_B) which will pass our analysis selection. We perform this estimation in each bin of hadron-jet-level dijet mass. It turns out that only the ratio of the forward to the backward acceptance affects the analysis, so we compute that ratio $R = \frac{\epsilon_F}{\epsilon_B}$. We also estimate the effect on this ratio of varying the scale and the jet energy scale.

To estimate the asymmetry at the hadron-jet level, we employ a Bayesian calculation using Markov Chain Monte Carlo provided by the PYMC [10] software package. We construct a statistical model for our data as follows.

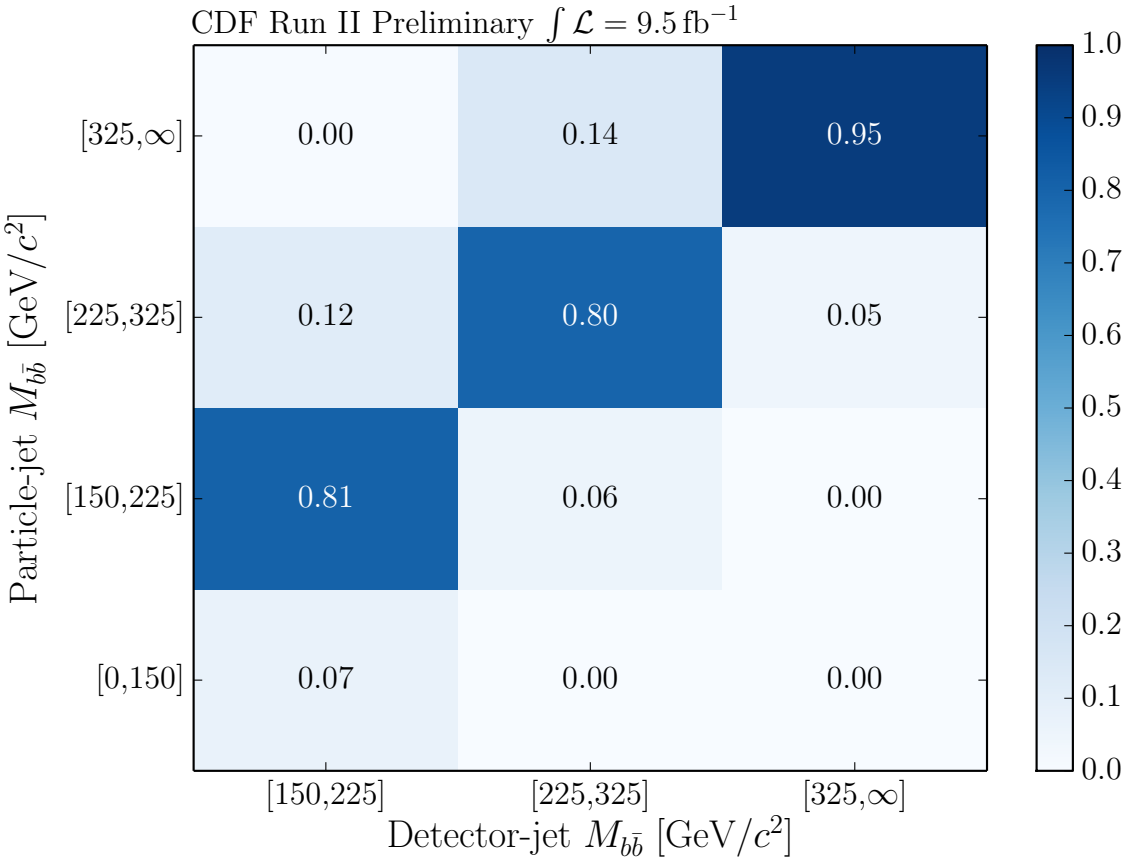

FIG. 4. The smearing matrix relating measured dijet mass to hadron-jet-level dijet mass

- f_{MQT} is the $b\bar{b}$ fraction in each bin of dijet mass (M), charge difference (Q), and tag-type (T). The prior probability distribution for f is a normal distribution centered at the calibrated value, with a width equal to the residual uncertainty from the calibration.

- P_{MQ} is the correct charge probability described in (13). The prior for $p_{0.5}$ and $p_{0.25}$ are a normal distributions with mean and uncertainty taken from the calibration.

- $F^{\mathrm{BG}}_{MQT}, B^{\mathrm{BG}}_{MQT}$ are the rate of forward and backward events in the background-dominated sideband. From these, we can calculate the background asymmetry, which we assume is the same in the signal region. The priors for these are the Poisson likelihood.

- J is the shift in the jet energy scale. We coherently shift all of the jet energies in every Monte Carlo event by J times the jet-energy uncertainty. The prior is a standard normal distribution.

- $S_{M'MQ}(J)$ is a matrix describing the contribution of events with hadron-jet-level dijet

mass M' to the various bins of measured dijet mass and charge difference. The matrix is a function of the jet energy scale shift, J. The prior is taken from the rate and uncertainty in Monte Carlo, and the matrix is normalized so that $\sum_{M'} S_{M'MQ}(J) = 1$.

- $\sigma_{M,Q,T}$ is the rate of events in each bin of detector-level $b\bar{b}$ mass, charge difference, and tag type. This has a uniform prior from zero to many times the actual number of observed events in the data. This is necessary because the Monte Carlo does not simulate b-tagging rates and efficiencies or charge differences perfectly.

- $R_{M'}$ is the ratio of the forward to the backward acceptance. The prior is a normal distribution with mean and width taken from the calibration described above.

- $A_{M'}$ is the $b\bar{b}$ asymmetry in bins of hadron-jet-level mass. This is the parameter we wish to measure. It has a flat prior from [-1, 1].

- $A^{\rm acc}_{M'}$ is the $b\bar{b}$ asymmetry after acceptance and selection effects. It is a deterministic function of $A_{M'}$ and $R_{M'}$:

$$A^{\rm acc}_{M'} = \frac{R_{M'}(1+A_{M'}) - (1-A_{M'})}{R_{M'}(1+A_{M'}) + (1-A_{M'})}.$$

From these parameters, we can compute the rate λ of forward and backward events in data, and compare this rate to our observed data via a Poisson likelihood (given an observation of k events):

$$L(\lambda|k) = \frac{\lambda^k e^{-\lambda}}{k!}.$$

The rates λ are

$$\lambda^{\rm Forward}_{MQT} = \Big[f^B_{MQT} \sum_{M'} \frac{1 + A^{\rm acc}_{M'}(2P_{MQ}-1)}{2} S_{M'MQ}(J) + (1 - f^B_{MQT}) \frac{F^{\rm BG}_{MQT}}{F^{\rm BG}_{MQT} + B^{\rm BG}_{MQT}} \Big] \times \sigma_{MQT}, \tag{14}$$

and

$$\lambda^{\rm Backward}_{MQT} = \Big[f^B_{MQT} \sum_{M'} \frac{1 - A^{\rm acc}_{M'}(2P_{MQ}-1)}{2} S_{M'MQ}(J) + (1 - f^B_{MQT}) \frac{B^{\rm BG}_{MQT}}{F^{\rm BG}_{MQT} + B^{\rm BG}_{MQT}} \Big] \times \sigma_{MQT}. \tag{15}$$

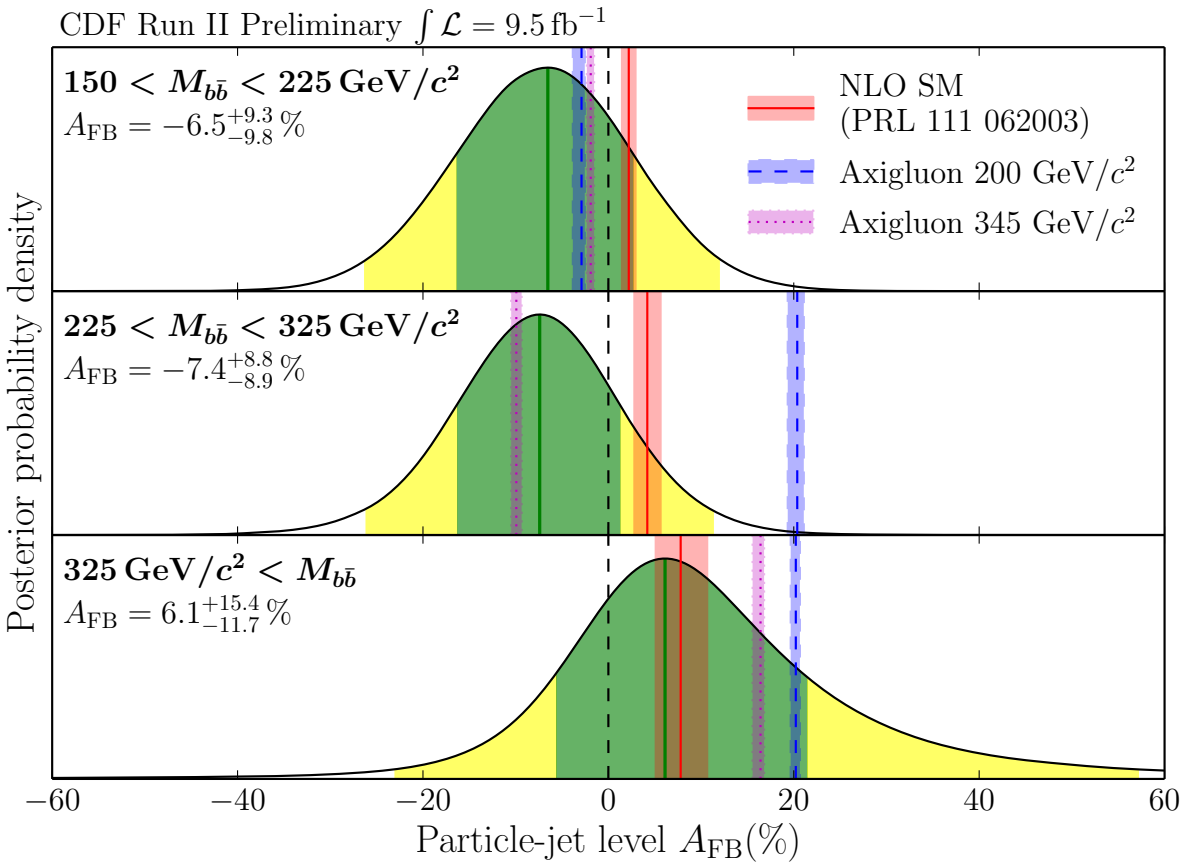

FIG. 5. Marginal posterior probability distribution of asymmetry in each bin of hadron-jet-level $b\bar{b}$ mass. The green and yellow bands represent the 68 % and 95 % credible intervals, respectively.

The prior probability densities described above, together with this likelihood, are sufficient under Bayes' theorem to fully specify the posterior probability density for the parameters. To estimate this posterior density, we employ Markov Chain Monte Carlo (MCMC), a common computational technique in Bayesian statistics. This technique provides us with samples from the posterior probability distribution over the parameter space. We marginalize the nuisance parameters, and obtain the posterior density for $A_{M'}$, the asymmetry in each bin of hadron-jet-level $b\bar{b}$ mass. The marginal distributions are shown in Figure 5.

V. RESULTS

To characterize the posterior and describe our measurement, we find the highest-probability-density credible intervals at 68 % and 95 % credibility for $A_{M'}$ in each hadron-jet-level mass

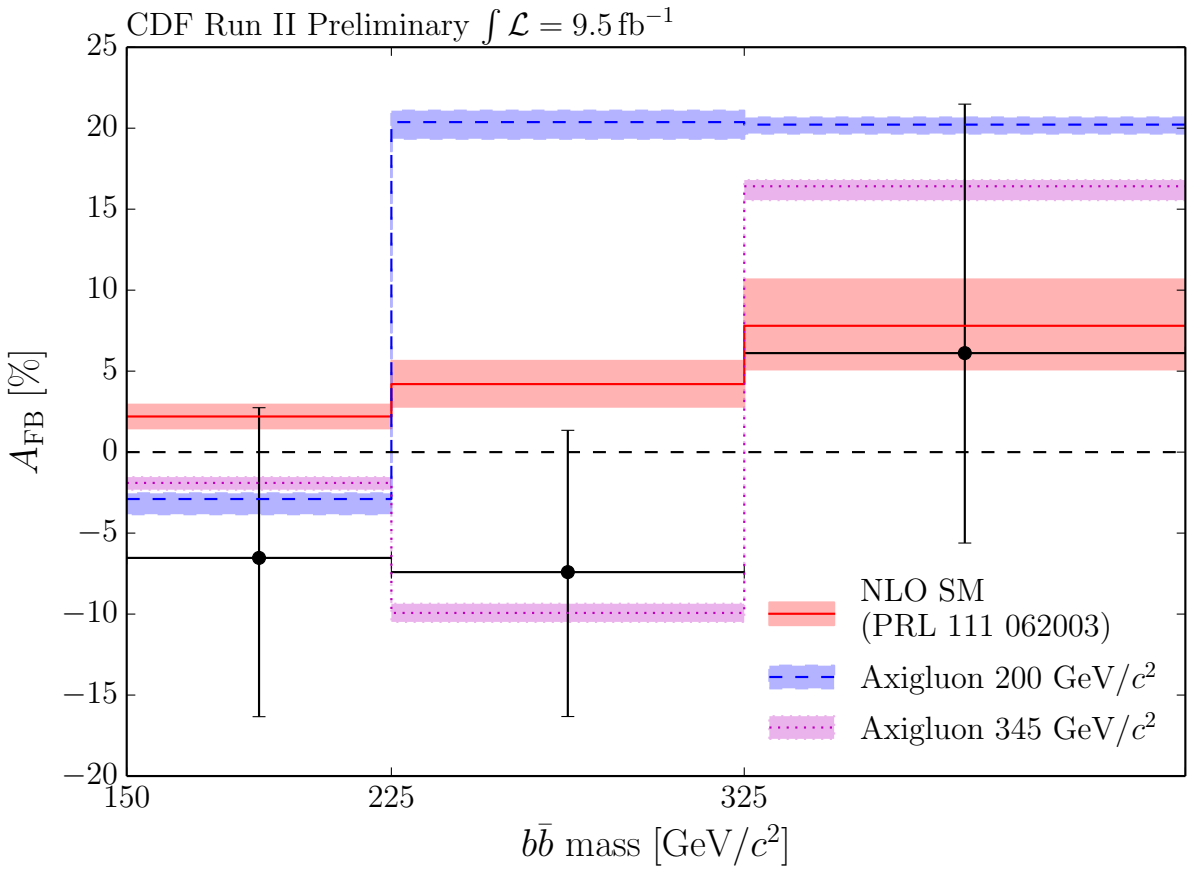

FIG. 6. Maximum a posteriori points for the signal asymmetry in each mass bin. The error bars represent the 68 % credible intervals.

bin. These posteriors, along with the 68 and 95 % credible intervals describing them, are shown in Figure 5. The red vertical bands represent the theoretical predictions from Table I. The results are consistent with zero and with the standard model prediction in each bin.

VI. CONCLUSION

We have measured the forward-backward asymmetry of $b\bar{b}$ pairs as a function of the mass of the $b\bar{b}$ pair. This measurement is corrected to the hadron-jet level, accounting for the effects of backgrounds, charge misidentification, mismeasurement, and non-uniform detector acceptance. We observe an asymmetry in each mass bin that is consistent with zero and consistent with the standard model prediction of Ref. [6]. We are able to exclude wide axigluons with a mass of 200 GeV c^{-2}, but not the heavier axigluon at 345 GeV c^{-2}. This

FIG. 7. Validation plots in the $150 < m_{b\bar{b}} < 225\,\mathrm{GeV}\,c^{-2}$ bin for all tag categories

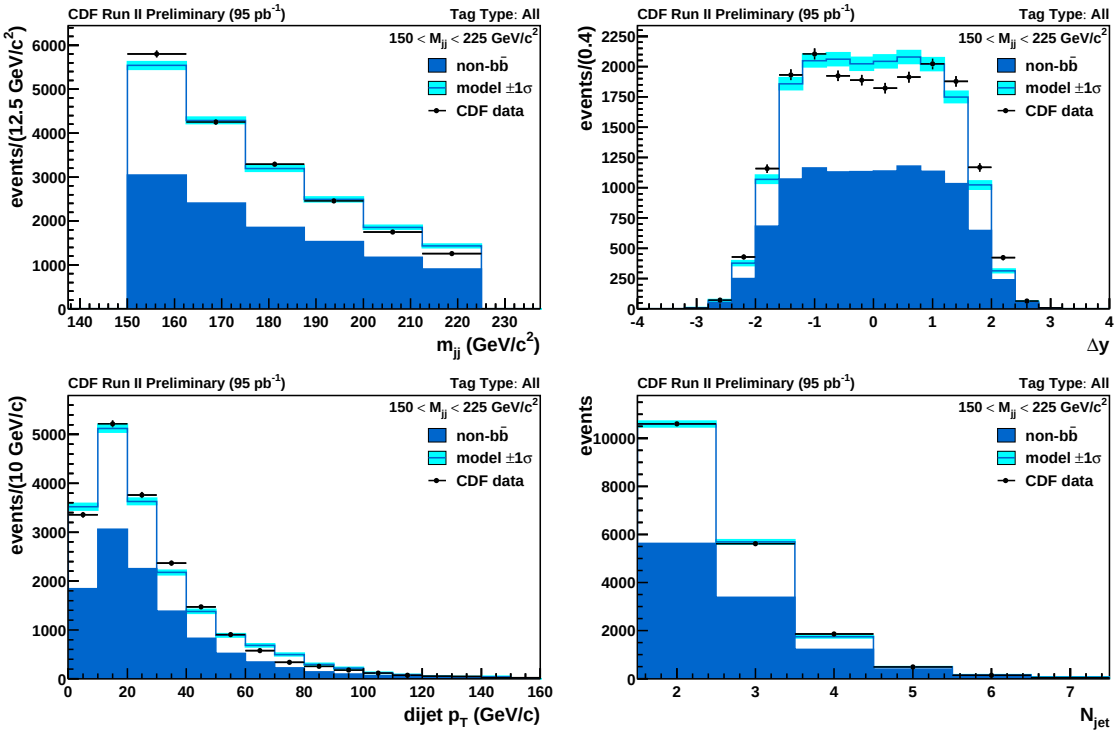

measurement slightly reduces the allowed parameter space for light axigluon models to explain the top quark forward-backward asymmetry.

Appendix A: Additional plots

In order to validate our MC model, we produced a number of plots of various kinematic quantities in the analysis subsamples. These can be seen in Figures 7-18. In each of these plots, the $b\bar{b}$ signal has been normalized to the calibrated $b\bar{b}$ fraction times the number of events, and the background has been normalized to one minus the $b\bar{b}$ fraction times the number of events.

[1] T. Aaltonen *et al.* (CDF Collaboration), Phys. Rev. D **87**, 092002 (2013); V. M. Abazov *et al.* (D0 Collaboration), Phys. Rev. D **84**, 112005 (2011).

[2] J. H. Kuhn and G. Rodrigo, Phys. Rev. Lett. **81**, 49 (1998).

FIG. 8. Validation plots in the $150 < m_{b\bar{b}} < 225\,\mathrm{GeV}\,c^{-2}$ bin for LL events

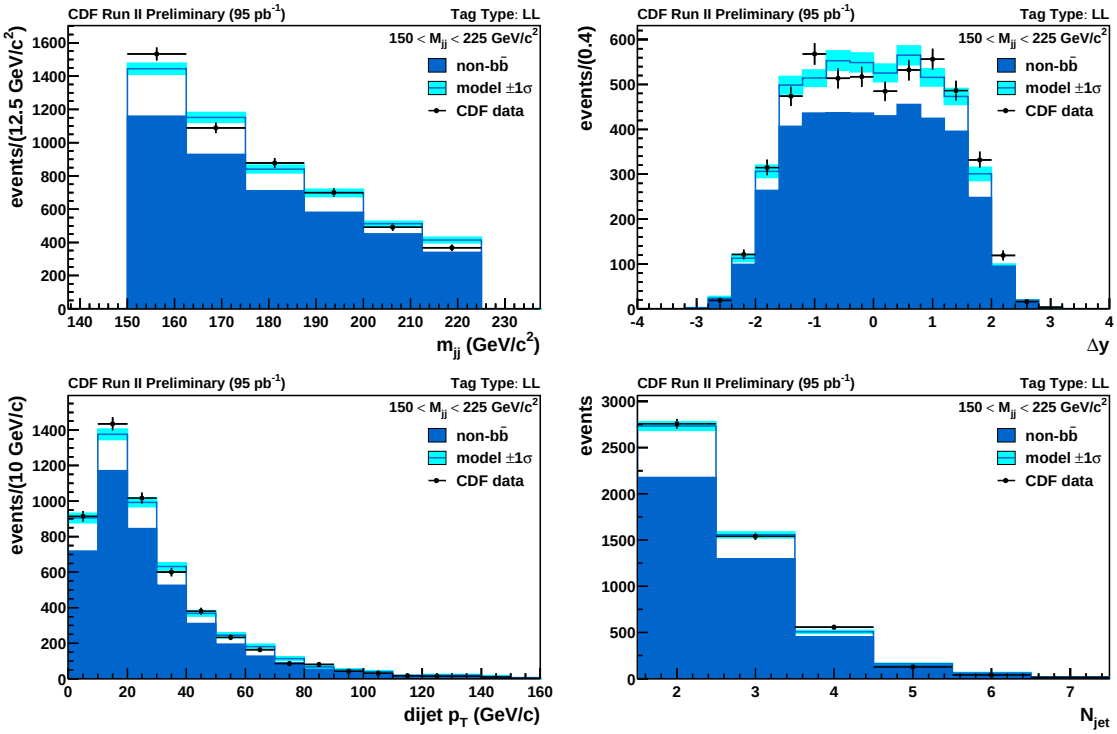

FIG. 9. Validation plots in the $150 < m_{b\bar{b}} < 225\,\mathrm{GeV}\,c^{-2}$ bin for LH events

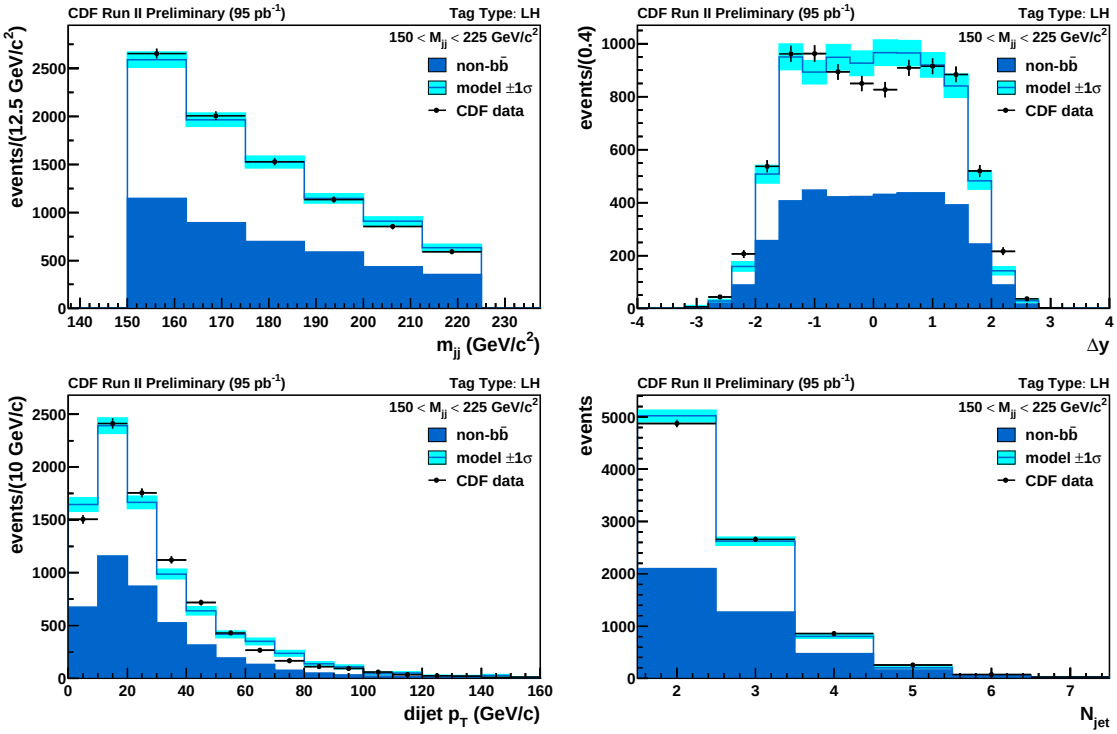

FIG. 10. Validation plots in the $150 < m_{b\bar{b}} < 225\,\mathrm{GeV}\,c^{-2}$ bin for HH events

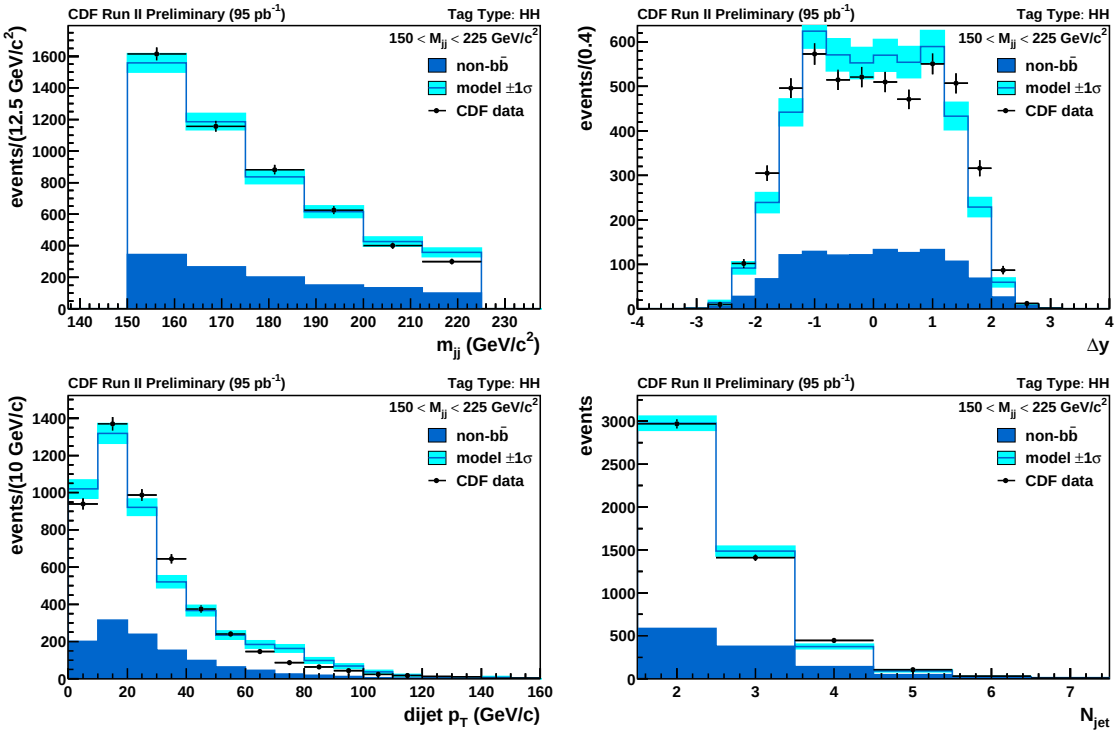

FIG. 11. Validation plots in the $225 < m_{b\bar{b}} < 325\,\mathrm{GeV}\,c^{-2}$ bin for all tag categories

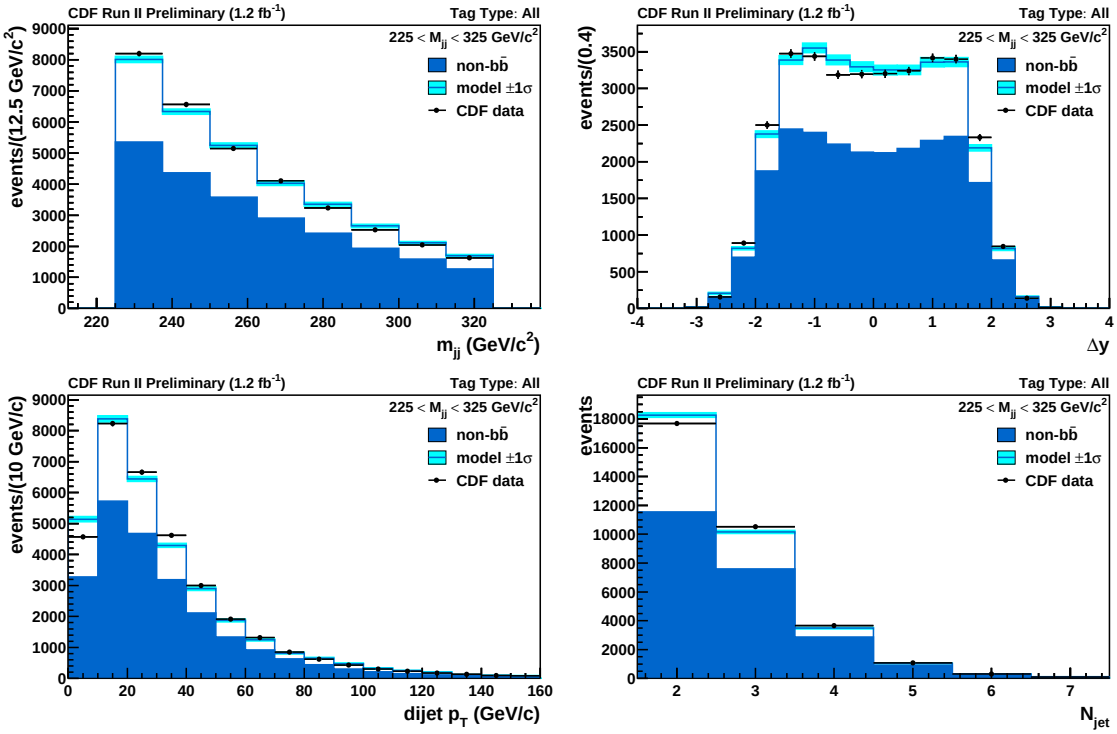

FIG. 12. Validation plots in the $225 < m_{b\bar{b}} < 325\,\mathrm{GeV}\,c^{-2}$ bin for LL events

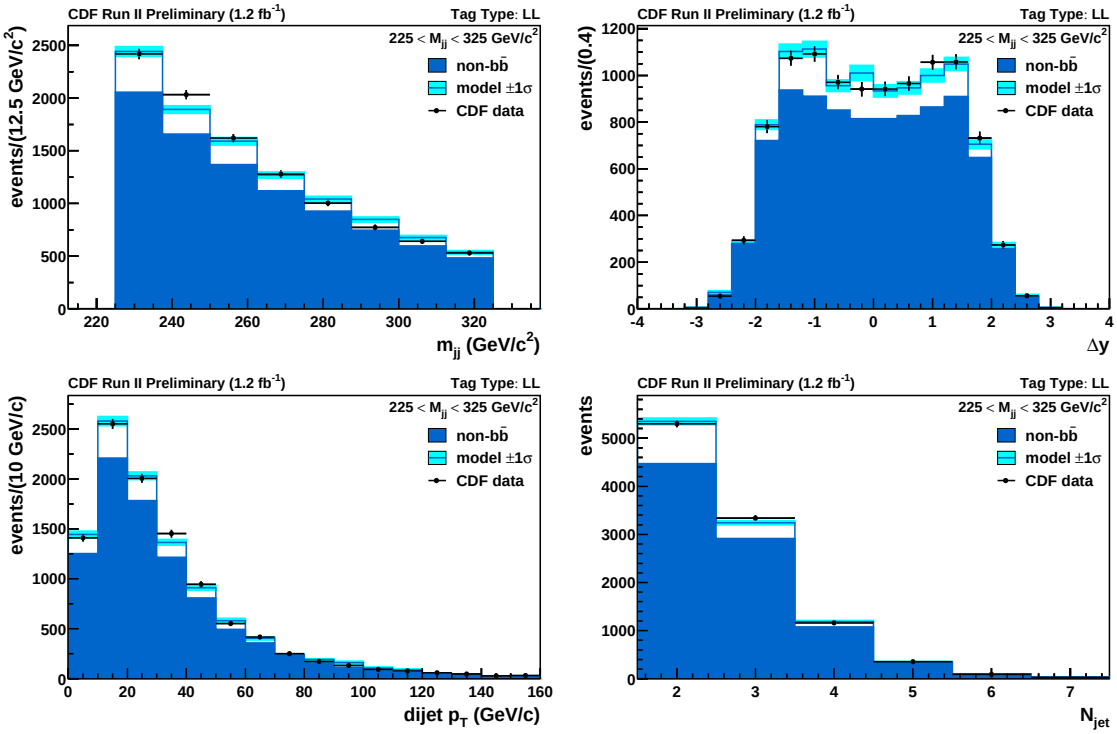

FIG. 13. Validation plots in the $225 < m_{b\bar{b}} < 325\,\mathrm{GeV}\,c^{-2}$ bin for LH events

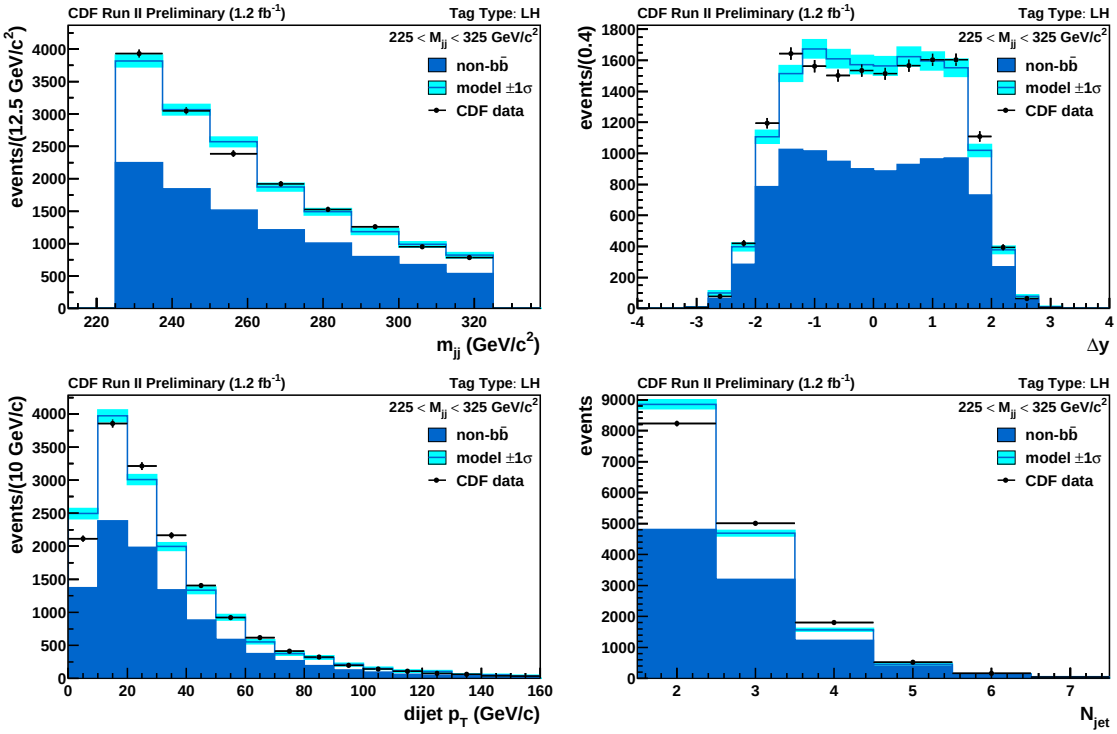

FIG. 14. Validation plots in the $225 < m_{b\bar{b}} < 325\,\mathrm{GeV}\,c^{-2}$ bin for HH events

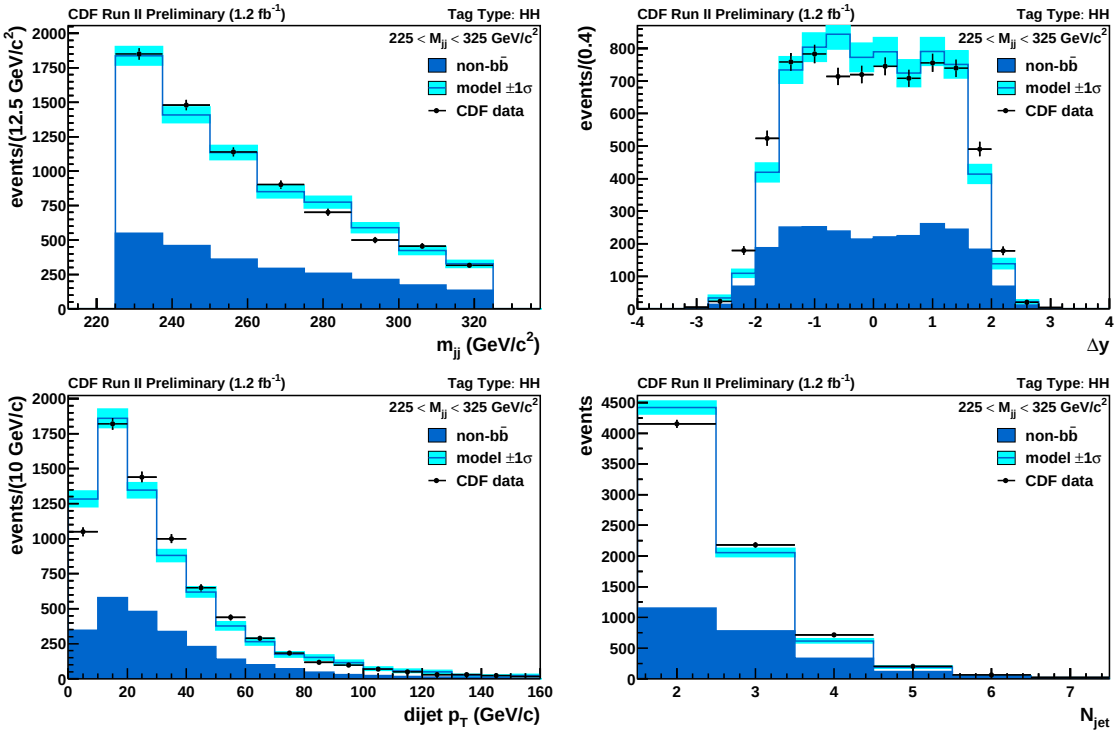

FIG. 15. Validation plots in the $m_{b\bar{b}} > 325\,\mathrm{GeV}\,c^{-2}$ bin for all tag categories

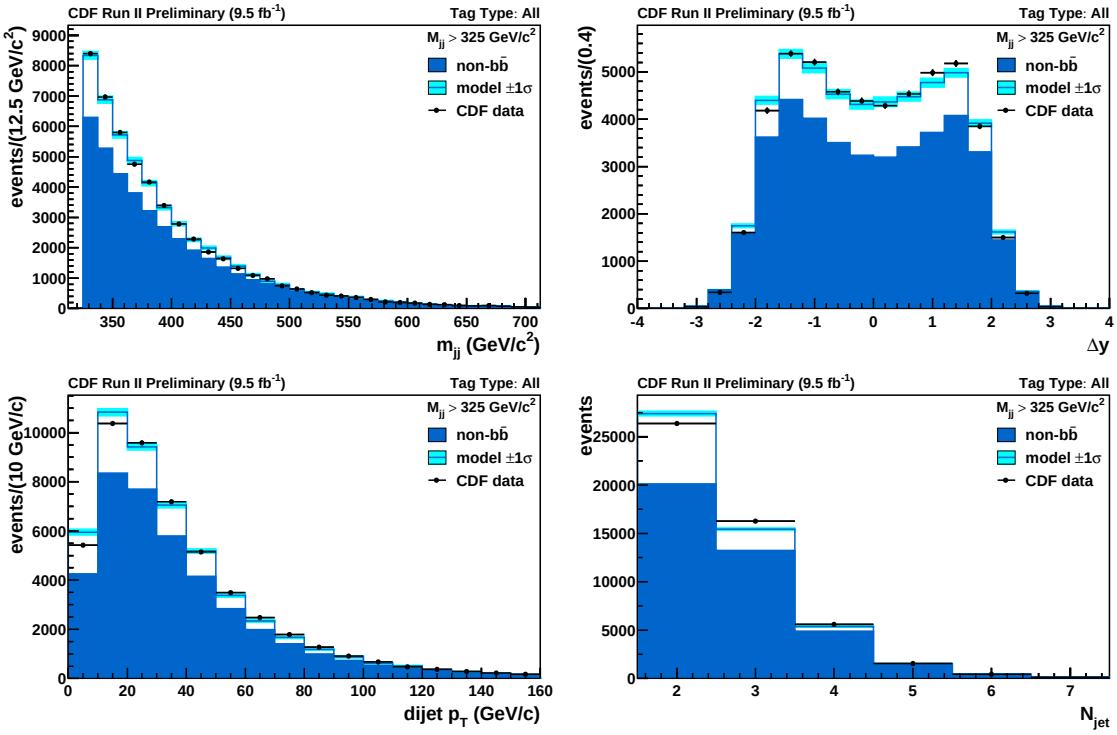

FIG. 16. Validation plots in the $m_{b\bar{b}} > 325\,\mathrm{GeV}\,c^{-2}$ bin for LL events

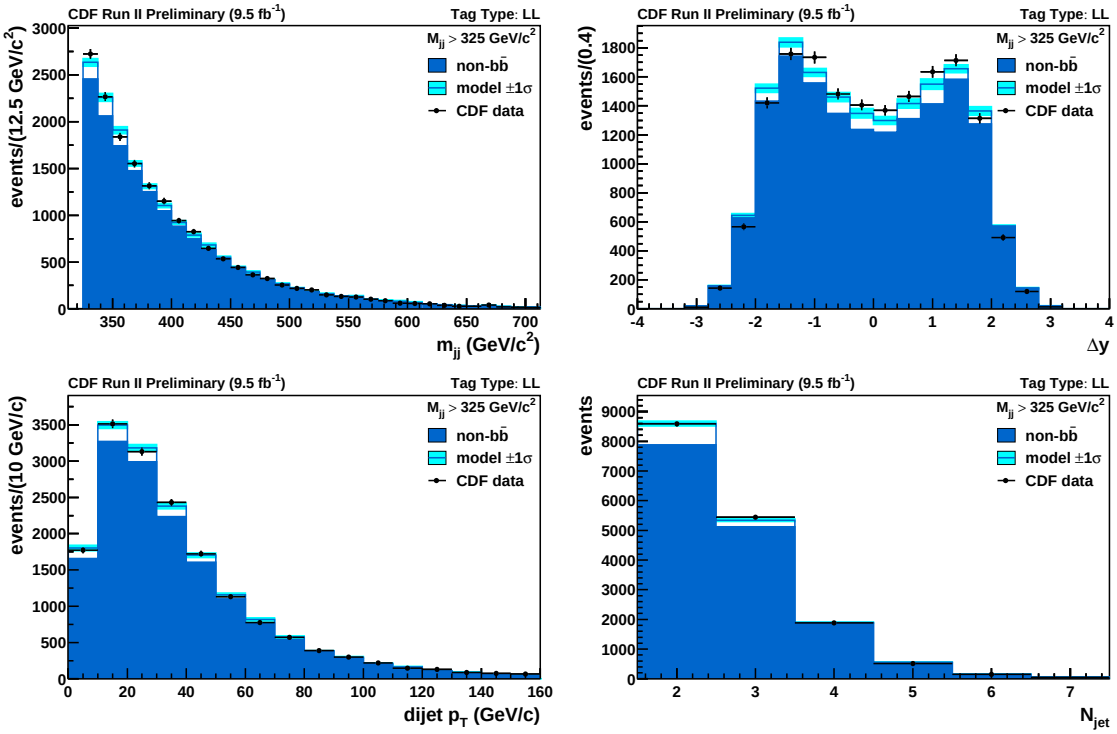

FIG. 17. Validation plots in the $m_{b\bar{b}} > 325\,\mathrm{GeV}\,c^{-2}$ bin for LH events

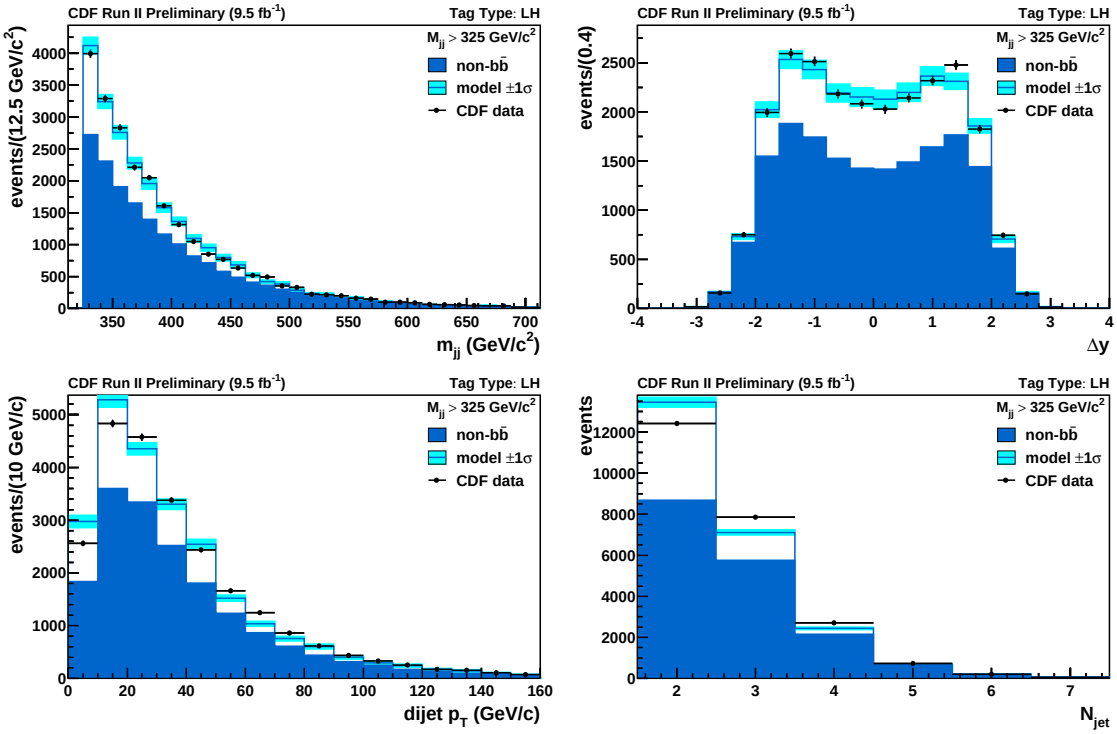

FIG. 18. Validation plots in the $m_{b\bar{b}} > 325\,\mathrm{GeV}\,c^{-2}$ bin for HH events

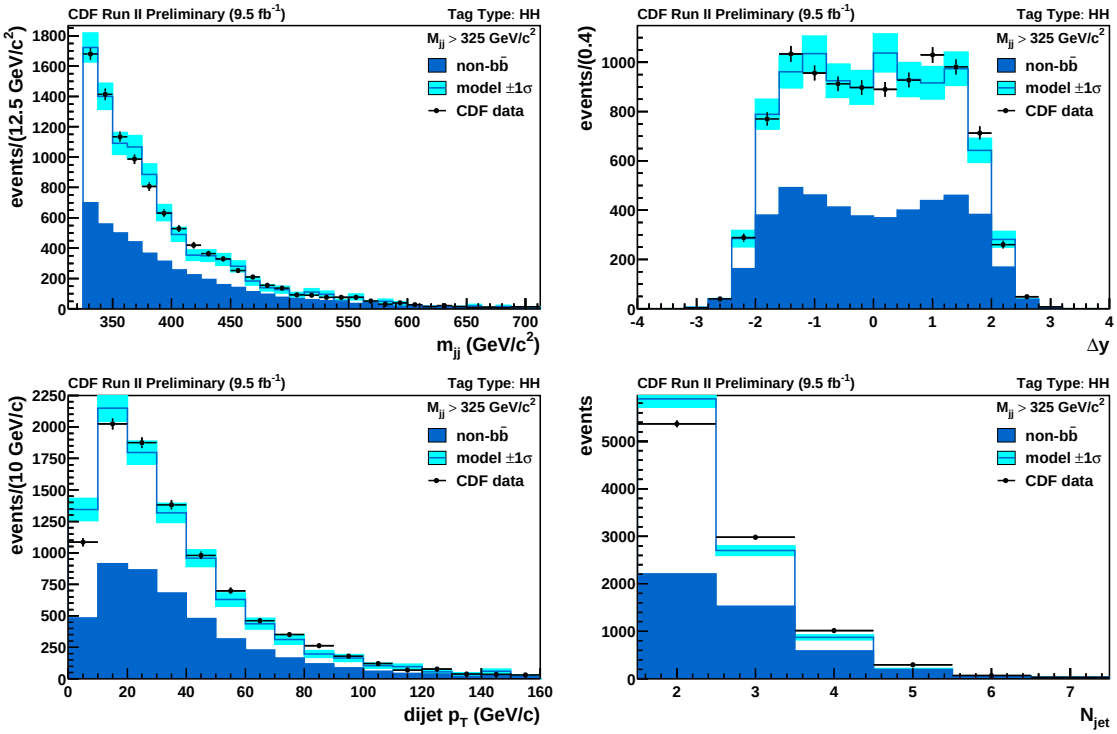

[3] W. Hollik and D. Pagani, Phys. Rev. D **84**, 093003 (2011); J. H. Kuhn and G. Rodrigo, J. High Energy Phys. **01**, 063 (2012); A. V. Manohar and M. Trott, Phys. Lett. B **711**, 313 (2012).

[4] M. I. Gresham, I.-W. Kim, and K. M. Zurek, Phys. Rev. D **83**, 114027 (2011); S. Jung, A. Pierce, and J. D. Wells, Phys. Rev. D **83**, 114039 (2011); J. F. Kamenik, J. Shu, and J. Zupan, Eur. Phys. J. C **72**, 2102 (2012).

[5] C. Gross, G. Marques Tavares, M. Schmaltz, and C. Spethmann, Phys. Rev. D **87**, 014004 (2013); A. Carmona, M. Chala, A. Falkowski, S. Khatibi, M. M. Najafabadi, *et al.*, "From Tevatron's top and lepton-based asymmetries to the LHC," (2014), arXiv:1401.2443 [hep-ph].

[6] B. Grinstein and C. W. Murphy, Phys.Rev.Lett. **111**, 062003 (2013), arXiv:1302.6995 [hep-ph].

[7] We use a fixed-size cone algorithm to identify jets with a cone size of 0.7 rad.

[8] D. Acosta *et al.* (CDF Collaboration), Phys. Rev. D **71**, 052003 (2005).

[9] Grinstein, G. da Costa, and Sherman, CDF/DOC/SEC_VTX/CDFR/8626.

[10] A. Patil, D. Huard, and C. J. Fonnesbeck, Journal of Statistical Software **35**, 1 (2010).